AIP | Applied Physics Letters

Phase separation and optical properties in oxygen-rich InN films

A. Dixit, C. Sudakar, R. Naik, G. Lawes, J. S. Thakur, E. F. McCullen, G. W. Auner, and V. M. Naik

Citation: Applied Physics Letters **93**, 142103 (2008); doi: 10.1063/1.2963498
View online: http://dx.doi.org/10.1063/1.2963498
View Table of Contents: http://scitation.aip.org/content/aip/journal/apl/93/14?ver=pdfcov
Published by the AIP Publishing

Phase separation and optical properties in oxygen-rich InN films

A. Dixit,[1] C. Sudakar,[1] R. Naik,[1] G. Lawes,[1,a)] J. S. Thakur,[2,b)] E. F. McCullen,[2] G. W. Auner,[2] and V. M. Naik[3]
[1]*Department of Physics and Astronomy, Wayne State University, Detroit, Michigan 48201, USA*
[2]*Department of Electrical and Computer Engineering, Wayne State University, Detroit, Michigan 48202, USA*
[3]*Department of Natural Sciences, University of Michigan-Dearborn, Dearborn, Michigan 48128, USA*

(Received 27 April 2008; accepted 27 June 2008; published online 7 October 2008)

We have investigated the properties of sputter deposited InN thin films prepared from an In-metal (InN-MT) and an In_2O_3 target (InN-OT). The excess oxygen present in the InN-OT films alters the microstructure by introducing additional disorder. Depth dependent x-ray photoelectron spectroscopy measurements indicate the presence of higher concentrations of oxygen in InN-OT. Raman spectra show evidence for the presence of an In_2O_3 secondary phase in both samples. Although the InN-OT film has a higher oxygen concentration, both films show similar electrical and optical properties. © *2008 American Institute of Physics*. [DOI: 10.1063/1.2963498]

The III-V nitrides are promising compounds for optoelectronic applications in the visible and near-ultraviolet wavelength range.[1,2] Among these systems, InN has been particularly widely studied because of its potential applications to high speed electronics, high efficiency multijunction solar cells, and other applications.[2] However, the presence of intrinsic structural defects and unintentional impurities greatly affects the properties and performance of group III nitride thin films.[3,4]

The presence of oxygen impurities is almost unavoidable in GaN, AlN, InN, and their alloys[5] and are partially responsible for the *n*-type behavior of the nitrides.[6] Westra *et al.*[7] studied the effects of oxygen contamination on the properties of reactively sputtered InN films, but despite a high O content, the samples showed no evidence of an In_2O_3 phase. They proposed that the oxygen impurities formed an amorphous indium oxynitride embedded in the polycrystalline InN matrix. These defects would act as additional scattering centers reducing the mobility and increasing the electron concentration.

Optical measurements on very high quality InN films[8,9] show a band gap in the range 0.7–0.9 eV (carrier concentration of $\sim 10^{17}-10^{18}$ cm^{-3}), which is significantly smaller than the typical values of 1.8–2.1 eV (carrier concentration of $\sim 10^{20}$ cm^{-3}) reported earlier in other samples. The larger band gap values have been attributed to the presence of oxynitrides formed by the incorporation of oxygen in InN (Refs. 10 and 11) or due to band filling effects in the highly degenerate InN samples.[3] Davydov *et al.*[11] showed that samples with band gaps in the range 1.8–2.1 eV contained up to 20% oxygen impurities, a much higher concentration than samples with narrow band gap values.

Motivated by the important role of oxygen impurities on the materials properties of InN, we have studied InN films prepared from In-metal (InN-MT) and In_2O_3 targets (InN-OT) to investigate how incorporating additional oxygen modifies the sample properties. We used a reactive rf magnetron sputtering system to deposit the samples onto (0001) sapphire substrates. The growth temperature of the samples was held at ~470 °C ± 5 °C. Both thin films were prepared with N_2, at a partial pressure of 5×10^{-3} torr, as the reactive gas and Ar as the sputtering gas at a working pressure of 1.5×10^{-2} torr. The final thickness for all samples was approximately 1 μm, as shown in the supplementary figure.[12] We used an oxide target to produce the oxygen-rich samples, because even a small concentration of reactive oxygen during sputtering, on the order of only 1%, give rise to highly crystalline textured In_2O_3 films rather than InN samples.

The x-ray diffraction (XRD) patterns for the InN films prepared from both the metal and the oxide targets are shown in Figs. 1(a) and 1(b). The InN-MT thin film shows intense peaks at $2\theta=31.43°$ and 65.4° corresponding to the (002) and (004) reflections for wurtzite InN, suggesting that the film is highly oriented. The InN-OT thin films showed broad reflections at $2\theta=28.96°$, 30.66°, and 32.85°, consistent with an isotropic polycrystalline sample. Using structure refinement, we determined the c/a axis ratios to be 1.611 and

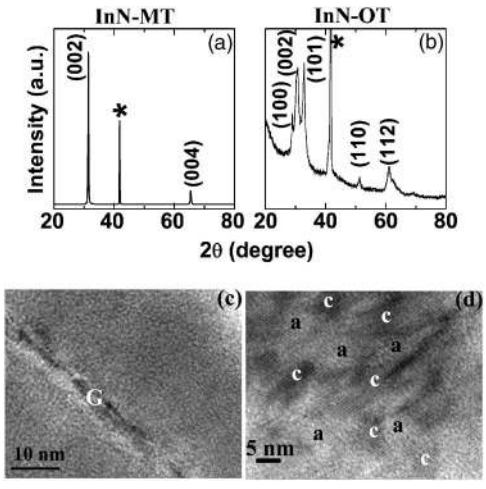

FIG. 1. XRD patterns of (a) InN-metal film and (b) InN-oxide film. The * indicates the substrate peak due to the Al_2O_3 (0006) reflection. HRTEM of (c) InN-metal and (d) InN-oxide thin films. In (c) "G" shows the grain-boundary region between the highly oriented InN columnar crystals. In (d) regions marked with letters "a" and "c" indicate the disordered amorphous and crystalline regions within the InN crystallites.

a)Electronic mail: glawes@wayne.edu.
b)Also at: Department of Physics and Astronomy, Wayne State University, Detroit, MI 48201.

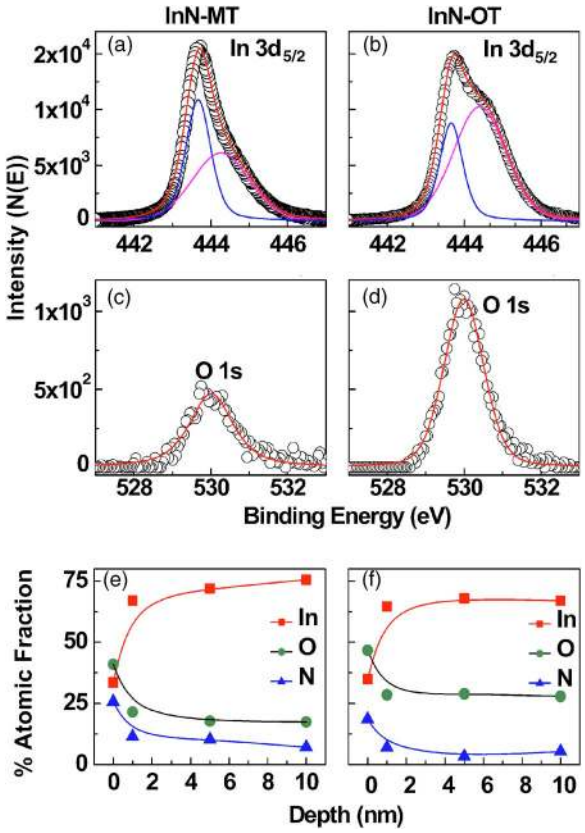

FIG. 2. (Color online) XPS spectra of In3$d_{5/2}$ after 10 nm etching for (a) InN-metal and (b) InN-oxide thin films. O1s electron spectra for the (a) and (b) are shown in (c) and (d). The concentration (at. %) of In, N, and O below the surface of (e) InN-metal and (f) InN-oxide films.

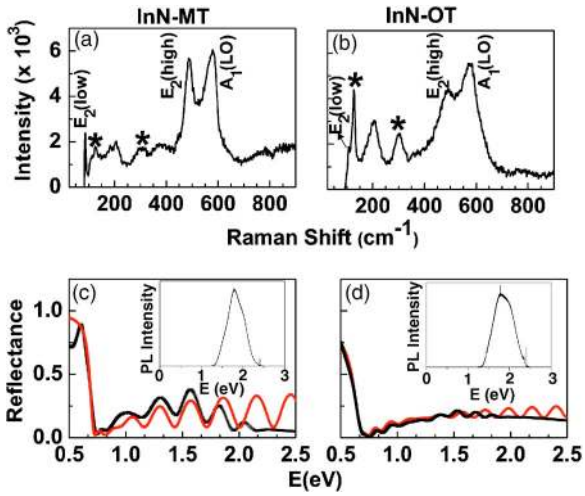

FIG. 3. (Color online) Raman spectra of (a) InN-metal and (b) InN-oxide thin films. The * corresponds to the peaks at 129 and 303 cm^{-1} modes (Ref. 21) from In_2O_3. Reflection spectra for InN films (a) and (b) are shown in (c) and (d). The solid curve is experimental data and the dashed curve is theoretical fit. The insets to (c) and (d) show the photoluminescence spectra, which exhibit broad peaks near 1.85 eV corresponding to the optical absorption edge of the samples. The sharp feature at 1.8 eV in the inset to (d) is due to the sapphire substrate, while the sharp peak at 2.4 eV is the residue left after filtering the laser line.

1.638 for the InN-MT and InN-OT films, respectively. The c/a ratio for the InN-MT film is very similar to the values previously reported,[13] while the large c/a ratio in the InN-OT film provides evidence for a large lattice distortion. We also carried out high resolution transmission electron microscopy (HRTEM) of these films. The InN-MT films show highly oriented columnar grains of the InN. These columnar structures are ~60 nm wide and ~1 μm long with the c-axis of the wurtzite structure perpendicular to the substrate plane. Highly crystalline columnar grains with no discernible defects are separated by grain boundaries [marked "G" in Fig. 1(c)]. Conversely, the InN-OT thin films have a number of defects beyond the grain-boundary regions [Fig. 1(d)]. These disordered/amorphous regions are marked by "a" and crystalline regions are labeled by "c." The crystalline regions are 5–8 nm in diameter.

We conducted x-ray photoelectron spectroscopy (XPS) studies using Al $K\alpha$ (1486.6 eV) radiation to probe the relative elemental concentrations of In, N, and O. An Ar^+ sputter etching process was used to carry out a depth profile elemental analysis. We measured three specific core-level spectra: In3$d_{5/2}$, N1s, and O1s, as shown in Fig. 2. The broad spectral features of In3$d_{5/2}$ spectrum can be deconvoluted into two peaks at 444.60 ± 0.02 eV and 443.50 ± 0.04 eV [Figs. 2(a) and 2(b)]. The peak at 443.50 ± 0.04 eV is assigned to the electron binding energy (BE) of In in InN while the higher energy peak at 443.50 ± 0.04 eV is attributed to the BE of In in In_2O_3 phase.[14,15] Both the InN-MT and InN-OT thin films have a high oxygen concentration at the surface and the spectrum (not shown) can be fitted with two peaks. We attribute the high BE peak at 532.00 ± 0.02 eV to adsorbed oxygen on the surface, which vanishes after Ar^+ removal of a 1 nm layer. The peak at 530 eV is invariant as a function of depth and can be associated with the BE of O, consistent with In–O coordination from an In_2O_3 secondary phase.[16] The amplitude of this peak in the InN-OT film is approximately twice that of the InN-MT film. The depth variation of the elemental concentrations is plotted in Figs. 2(e) and 2(f). The main nitrogen peak occurs at 396.40 ± 0.04 eV, with a low intensity peak at ~403.8 eV in the InN-MT film (not shown). This peak can be attributed to a N–O complex or N_2 molecule[17] and is observed only on the surface of the films. The decreasing N/In ratio on sputtering can be attributed to the small binding energy of N to In, which leads to the preferential removal of N during sputtering.[18]

Raman spectra for both samples are shown in Figs. 3(a) and 3(b). Both InN-MT and InN-OT films show the expected E_2(low), E_2(high), and A_1(LO) modes near 90, 490, and 580 cm^{-1}, respectively, indicating a preferred c-axis orientation for the InN crystallites. In addition to the InN modes, the spectra exhibit peaks at ~128, 305, and 370 cm^{-1} (marked with asterisk), which are characteristic of bcc-structured In_2O_3.[10,19,20] Further, an unassigned phonon mode ~200 cm^{-1} is present in the Raman spectra of both films with enhanced intensity in the InN-OT sample. This band could be a disorder activated mode. It is interesting to note that an infrared active phonon mode of In_2O_3 (Ref. 21) is observed at 218 cm^{-1}, consistent with a possible violation of the Raman selection rules in this sample. Further, the presence of other In_2O_3 modes (at 471, 504, and 630 cm^{-1})[22] with significant intensity could broaden the E_2(high) and A_1(LO) phonon modes in InN. These Raman studies confirm the presence of an In_2O_3 secondary phase in both samples.

In order to investigate the effect of oxygen concentration on the electrical and optical properties of the InN-MT and InN-OT films, we have performed Hall effect, optical transmission/reflection, and photoluminescence (PL) mea-

surements at 300 K. Hall effect measurements yield a carrier concentration of $\sim(9\pm1)\times10^{20}$ cm^{-3} and $(9\pm0.5)\times10^{20}$ cm^{-3} for InN-MT and InN-OT films, respectively. The carrier concentration is similar in both films, despite the fact that the InN-OT sample has twice the oxygen concentration of the InN-MT film. We have analyzed the reflectance spectra [Figs. 3(c) and 3(d)] with the Drude model,[23,24] using the plasmon frequency (ω_p) and the damping constant (γ) as fitting parameters. We used a value of 7.5 for the high frequency dielectric (ε_∞) constant; although ε_∞ for InN is not firmly established[25] the range of values reported in literature varies from 5.8 to 9.3.[26] However, the quality of the fits is not drastically affected by these different values of ε_∞. We find that $\omega_p\sim0.7$ eV for both the films, which have different values of γ (0.043 eV for InN-MT and 0.087 eV for InN-OT). PL emission spectra [insets in Figs. 3(c) and 3(d)] also show strong and broad peaks centered at ~1.85 eV for both samples. We determined the optical absorption edge using plots of $(\alpha\cdot E)^2$ versus photon energy (not shown) yield an absorption edge (E_a) of $\sim1.8-2.0$ eV for InN-OT and InN-MT films.

These measurements suggest that these sputter deposited InN films develop an In_2O_3 secondary phase when sufficiently high concentration of oxygen is present in the sample. At low concentrations, the oxygen atoms are likely to form point defects distributed homogeneously throughout the InN lattice.[4,8] The total energy to form an oxygen defect includes contributions from the structural relaxation energy, the local chemical energy, and the energy required to add an additional electron to the conduction band. The first two terms are approximately independent of oxygen concentration for small concentrations. However, each additional oxygen atom changes the electron chemical potential by injecting an additional electron into the conduction band. At higher impurity concentrations, the energy cost to incorporate oxygen as point defects can become very high, leading to the development of a secondary phase. Our measurements suggest that under certain conditions this secondary phase could be In_2O_3, in addition to the InN_xO_y secondary phase previously discussed.[13] The In_2O_3 secondary phase appears to nucleate along grain boundaries in higher quality InN samples, but can be distributed more homogeneously in disordered samples, as well as at grain boundaries, as observed in the InN-OT films. Oxygen in an In_2O_3 secondary phase will not donate electrons and thus will not increase the carrier concentration. This is consistent with our observation that the In-MT and In-OT films have very similar optical properties, despite the fact that the O concentration in the latter film is almost a factor of 2 larger.

In summary we investigated the effects of incorporating a high concentration of impurity oxygen on the properties of sputtered InN films fabricated using In and In_2O_3 targets. XPS measurements show that the oxygen concentration in the films prepared from the oxide target is double that of the samples prepared from the metal target, but both display an In_2O_3 secondary phase as confirmed by Raman spectroscopy. We surmise that this secondary oxide phase is predominantly localized in the grain-boundary region in the InN-metal films and is also located in the disordered/amorphous regions within InN crystallites in the InN-OT films. Optical characterization shows that both samples have similar carrier concentrations, confirmed by Hall measurements, and optical reflectance. These results suggest that beyond a certain concentration of oxygen, the oxygen-rich InN lattice becomes unstable with respect to the formation of an In_2O_3 impurity phase although the electrical properties of the films remain approximately unchanged.

This work is supported by the Institute for Manufacturing Research and the Center for Smart Sensors and Integrated Microsystems at Wayne State University.

[1] A. G. Bhuiyan, A. Hashimoto, and A. Yamamoto, J. Appl. Phys. **94**, 2779 (2003).
[2] S. Nakamura, M. Senoh, S. Nagahama, N. Iwasa, T. Yamada, T. Matsushita, H. Kiyoku, and Y. Sugimoto, Jpn. J. Appl. Phys., Part 2 **35**, L74 (1996).
[3] J. S. Thakur, Y. V. Danylyuk, D. Haddad, V. M. Naik, R. Naik, and G. W. Auner, Phys. Rev. B **76**, 035309 (2007).
[4] J. S. Thakur, R. Naik, V. M. Naik, D. Haddad, G. W. Auner, H. Lu, and W. J. Schaff, J. Appl. Phys. **99**, 023504 (2006).
[5] I. Shalish, Y. Shapira, L. Burstein, and J. Salzman, J. Appl. Phys. **89**, 390 (2001).
[6] M. D. McCluskey, N. M. Johnson, C. G. Van de Walle, D. P. Bour, M. Kneissl, and W. Walukiewics, Phys. Rev. Lett. **80**, 4008 (1998).
[7] K. L. Westra, R. P. W. Lawson, and M. J. Brett, J. Vac. Sci. Technol. A **6**, 1730 (1988).
[8] V. Y. Davydov, A. A. Klochikhin, R. P. Seisyan, V. V. Emptsev, S. V. Ivanov, F. Bechstedt, J. Furthmuller, H. Harima, A. V. Mudryi, J. Aderhold, O. Semchinova, and J. Garul, Phys. Status Solidi B **229**, R1 (2002).
[9] J. Wu, W. Walukiewicz, K. M. Yu, J. W. Ager III, E. E. Haller, H. Lu, W. J. Schaff, Y. Saito, and Y. Nanishi, Appl. Phys. Lett. **80**, 3967 (2002).
[10] E. Kurimoto, M. Hangyo, H. Harima, M. Yoshimoto, T. Yamaguchi, T. Araki, and Y. Nannishi, Appl. Phys. Lett. **84**, 212 (2004).
[11] V. Yu. Davydov, A. A. Klochikhin, V. V. Emtsev, D. A. Kurdyukov, S. V. Ivanov, V. A. Vekshin, F. Bechstedt, J. Furthmuller, J. Aderhold, J. Graul, A. V. Mudryi, H. Harima, A. Hashimoto, A. Yamamoto, and E. E. Haller, Phys. Status Solidi B **234**, 787 (2002).
[12] See EPAPS Document No. E-APPLAB-93-040830 for additional SEM and TEM images of the samples. For more information on EPAPS, see http://www.aip.org/pubservs/epaps.html.
[13] K. S. A. Butcher and T. L. Tansley, Superlattices Microstruct. **38**, 1 (2005).
[14] Q. X. Guo, M. Nishio, H. Ogawa, A. Wakahara, and A. Yoshida, Phys. Rev. B **58**, 15304 (1998).
[15] L. F. J. Piper, T. D. Veal, M. Walker, I. Mahboob, C. F. McConville, H. Lu, and W. J. Schaff, J. Vac. Sci. Technol. A **23**, 617 (2005).
[16] M. Faur, M. Faur, D. T. Jayne, M. Goradia, and C. Goradia, Surf. Interface Anal. **15**, 641 (1990).
[17] K. S. A. Butcher, A. J. Fernandes, P. P. T. Chen, M. Wintrebert-Fouquet, H. Timmers, S. K. Shrestha, H. Hirshy, R. M. Perks, and B. F. Usher, J. Appl. Phys. **101**, 123702 (2007).
[18] L. Cao, Z. L. Xie, B. Liu, X. Q. Xiu, R. Zhang, and Y. D. Zheng, J. Vac. Sci. Technol. B **25**, 199 (2007).
[19] M. Rojas-López, J. Nieto-Navarro, E. Rosendo, H. Navarro-Contreras, and M. A. Vidal, Thin Solid Films **379**, 1 (2000).
[20] C. Vigreux, L. Binet, and D. Gourier, J. Solid State Chem. **157**, 94 (2001).
[21] W. B. White and V. G. Keramidas, Spectrochim. Acta, Part A **28**, 501 (1972).
[22] A. Prim, E. Pellicer, E. Rossinyol, F. Peiró, A. Cornet, and J. R. Morante, Adv. Funct. Mater. **17**, 2957 (2007).
[23] I. Hamberg and C. G. Granqvist, J. Appl. Phys. **60**, R123 (1986).
[24] J. S. Thakur, G. W. Auner, D. B. Haddad, R. Naik, and V. M. Naik, J. Appl. Phys. **95**, 4795 (2004).
[25] A. Kasic, M. Schubert, Y. Saito, Y. Nanishi, and G. Wanger, Phys. Rev. B **65**, 115206 (2002).
[26] S. Rumyantsev, M. Shur, and M. Levinshtein, Int. J. High Speed Electron. Syst. **14**, 1 (2004).